

The Combined Sensor Program: An Air–Sea Science Mission in the Central and Western Pacific Ocean



Madison J. Post,* Christopher W. Fairall,* Jack B. Snider,+ Yong Han,+ Allen B. White,+
Warner L. Ecklund,+ Klaus M. Weickmann,# Patricia K. Quinn,@ Daniel I. Cooper,&
Steven M. Sekelsky,** Robert E. McIntosh,** Peter Minnett,++ and Robert O. Knuteson###

ABSTRACT

Twelve national research organizations joined forces on a 30-day, 6800 n mi survey of the Central and Tropical Western Pacific on NOAA's Research Vessel *Discoverer*. The Combined Sensor Program (CSP), which began in American Samoa on 14 March 1996, visited Manus Island, Papua New Guinea, and ended in Hawaii on 13 April, used a unique combination of in situ, satellite, and remote sensors to better understand relationships between atmospheric and oceanic variables that affect radiative balance in this climatically important region. Besides continuously measuring both shortwave and longwave radiative fluxes, CSP instruments also measured most other factors affecting the radiative balance, including profiles of clouds (lidar and radar), aerosols (in situ and lidar), moisture (balloons, lidar, and radiometers), and sea surface temperature (thermometers and Fourier Transform Infrared Radiometers). Surface fluxes of heat, momentum, and moisture were also measured continuously. The Department of Energy's Atmospheric Radiation Measurement Program used the mission to validate similar measurements made at their CART site on Manus Island and to investigate the effect (if any) of large nearby landmasses on the island-based measurements.

1. Introduction

The most quantitative statement of our accumulated knowledge about the climate system is the climate model or the general circulation model (GCM). The shortcomings of today's GCMs have been recently evaluated by Browning (1994). One major shortcoming is our insufficient understanding of the

interaction between clouds and the earth's radiation field. Clearly, there are important but poorly understood feedbacks between the direct warming effects from an increased greenhouse gas concentration and the indirect effects on global temperature from the resulting changes in cloud distributions and types. Another related factor is the complex role of air–sea interaction, in which clouds are a critical process. Marine clouds are dynamically, structurally, and microphysically distinct from continental clouds. Marine boundary layer (MBL) clouds strongly influence global climate because their relatively high albedos (compared with the ocean background) give rise to large deficits in absorbed solar radiative flux at the top of the atmosphere, while their low altitude prevents significant compensation in thermal emission (Randall et al. 1984). Deep convective clouds common in the western Pacific create profound reductions of the radiation reaching the surface; surface solar flux levels in the Tropics can be significantly lower than those in, say, Buffalo, New York, in December. Tropical deep convection also generates huge areas of cirrus clouds whose effect on net cloud forcing is still uncertain. For example, consider the recent debate about possible

*NOAA Environmental Technology Laboratory, Boulder, Colorado.

+Cooperative Institute for Research in the Environmental Sciences, University of Colorado, Boulder, Colorado.

#NOAA Climate Diagnostic Center, Boulder, Colorado.

@Pacific Marine Environmental Laboratory, Seattle, Washington.

&Los Alamos National Research Laboratory, Los Alamos, New Mexico.

**University of Massachusetts, Amherst, Massachusetts.

++University of Miami, Miami, Florida.

###University of Wisconsin—Madison, Madison, Wisconsin.

Corresponding author address: Madison J. Post, NOAA/ERL, R/E/ET4, 325 Broadway, Boulder, CO 80303.

E-mail: mpost@etl.noaa.gov

In final form 12 August 1997.

©1997 American Meteorological Society

cloud radiative flux absorption being significantly greater than that represented by present models (Cess et al. 1995; Chou et al. 1995; Evans et al. 1995; Ramanathan et al. 1995). This issue is particularly critical in the Tropics where clouds are thick and the solar flux is highest.

In the last decade, a number of research programs have focused on various aspects of this marine problem. For example the National Aeronautics and Space Administration (NASA) First International Satellite Cloud Climatology Program (ISCCP) Regional Experiment (FIRE) has executed a series of experiments in midlatitudes to investigate the role of cirrus and MBL stratus clouds in the climate system (Randall et al. 1984; Albrecht et al. 1988, 1995). In the near future, FIRE will venture to the Arctic to study stratus clouds of all types. The Tropical Oceans Global Atmosphere (TOGA) program conducted an extensive Coupled Ocean–Atmosphere Response Experiment (COARE) in the tropical western Pacific Ocean in 1992–93 (Webster and Lukas 1992). COARE focused on air–sea fluxes and the role of deep convection and larger-scale coupled interactions in short-term climate variability (primarily El Niño). The pivotal role of the western Pacific “boiler box” in global climate has been emphasized by recent debates about the importance of radiative flux and oceanic surface temperature coupling, a phenomenon usually referred to as the thermostat hypothesis (Zhang et al. 1995). This issue was examined (Zhang and Grossman 1996) in the Central Equatorial Pacific Experiment (CEPEX), which followed immediately after COARE.

In recognition of the need for a different experimental approach to climate problems (both marine and continental), the Department of Energy (DOE) initiated the Atmospheric Radiation Measurement (ARM) program (Stokes and Schwartz 1994). The heart of the ARM program is the development of several Cloud and Radiation Testbed (CART) remote-sensing facilities as experimental analogs of a GCM grid cell. A second element of ARM involves participation in intensive field studies to improve and test sensors and to investigate physical processes in more detail. ARM has identified the Southern Great Plains (SGP), the North Slope of Alaska (NSA), and the Tropical Western Pacific (TWP) climate regimes for installation of CART sites. The SGP site is currently fully operational; the other two sites are not yet fully instrumented. The ARM TWP effort has issues in common with those of COARE (the role of air–sea interaction processes in interannual climate variability) and FIRE

(the representation of clouds in climate models with an emphasis on satellite linkages), but its focus on local but long-term remote and in situ measurements is quite different.

The development of the CART instrument systems for the TWP is under way; however, their deployment in oceanic locations presents special problems. For instance, the harsh marine environment typically takes a great toll on sensors; an island may impart unknown distortions to measured profiles; and systems mounted on ships may require very demanding motion corrections. Current plans for TWP CART sites call for several surface-based remote-sensing packages, Atmospheric Radiation and Cloud Stations (ARCS), to be deployed on islands in the western Pacific. The need and practicality of a purely ocean-based (ship or buoy) site is still being debated. Clearly, an oceanic deployment will eliminate the uncertain complications from island-generated perturbations to the flow and the resulting changes to the clouds, but the logistics and costs may be prohibitive. The information required to make thoughtful choices is simply unavailable.

To attack this problem, we proposed to draw on extensive experience at the National Oceanic and Atmospheric Administration (NOAA) Environmental Technology Laboratory (ETL) in making marine atmospheric measurements. The ETL effort began with ship-based direct measurements of air–sea fluxes in the COARE pilot cruise in the equatorial Pacific in 1990 (Young et al. 1992) and with our first efforts at remote sensing with a ceilometer and a stabilized Doppler wind-profiling radar in the equatorial eastern Pacific in 1991 during the Tropical Instability Wave Experiment (TIWE; Chertock et al. 1993). This same system was deployed in the Azores region in 1992 as part of the Atlantic Stratocumulus Transition Experiment (ASTEX; White et al. 1995); land-based remote sensors were also deployed on an island (Frisch et al. 1995). The complete system was deployed on three cruise legs in the TWP during COARE (Young et al. 1995; Fairall et al. 1996a). Details on the instruments and techniques used in these and subsequent efforts can be found in Fairall et al. (1997).

Besides ETL’s interest in climate and forecasting issues in marine meteorology, both the NOAA National Environmental Satellite, Data and Information Service (NESDIS) and NOAA Corps (uniformed organization established to operate NOAA’s fleet of ships and aircraft) were interested in developing capabilities to equip a few NOAA research vessels with a suite of in situ and remote sensors. This would help

NESDIS better calibrate and validate satellite data products, help NOAA's National Weather Service (NWS) fill in data voids over the oceans to improve numerical weather prediction, and provide valuable, quasi-operational research data to the climate modeling community. With the support of these organizations, 30 days of ship time for the first year of the plan, 1996, were requested and allocated on NOAA R/V *Discoverer*.

The Combined Sensor Program (CSP), a joint NOAA-DOE effort, was thus established to promote seagoing climate research and as a continuation of the ongoing island and ship-based studies. We then developed a plan to conduct a cruise to the TWP aboard the NOAA ship *Discoverer*, which was instrumented with the most advanced in situ and remote sensors in the ETL inventory, supplemented by sensors from a number of universities and government laboratories active in the ARM program. Several investigators from the Aerosol Characterization Experiment (ACE) and the World Ocean Circulation Experiment (WOCE) that preceded CSP were invited to leave some of their instrumentation on board the *Discoverer* and join CSP, providing aerosol and air-ocean chemistry measurements and direct satellite reception. Thus, the inventory of measurements for this cruise far exceeded any of ETL's previous efforts.

Besides the obvious opportunity to address the numerous ARM scientific issues discussed above, this field program was also intended to provide an opportunity for ARM to gain further experience with shipboard remote sensing of clouds that might be useful in the development of TWP CART facilities. The scientific goal of the CSP mission thus evolved to "obtain an unprecedented dataset on marine clouds and radiation" in the central and western tropical Pacific by deploying a suite of ship-based sensors on a 30-day mission. It was also to develop "improved analysis techniques and improved cloud-radiative interaction parameterizations and cloud dynamical models, and to evaluate cloud effects on the surface energy budget of the tropical western Pacific (TWP)." Implicitly, another goal was to help establish whether the island-based measurements could be considered representative of the region, including the open ocean, or if they were influenced by nearby landmasses. Thus, our intention was to deploy a ship-based system functionally equivalent to various components of a prototype ARCS system and to compare our shipboard measurements with those from similar island-based sensors in the prototype ARCS system operated by The Pennsyl-

vania State University and the ARM TWP team at Manus Island in Papua New Guinea.

To satisfy these goals, we planned to gather data to 1) parameterize cloud-aerosol-radiation interactions in a tropical marine environment; 2) improve parameterizations of surface fluxes of heat, momentum, and moisture; 3) determine cloud cover and cloud layering statistics in the TWP; 4) evaluate marine boundary layer height and internal characterization; 5) characterize TWP stratus and cumulus clouds in terms of radiative effects, ice and water mass, and effective radii; 6) validate aerosol and radiance data from polar-orbiting satellites; 7) characterize the effects of the MBL on measurements of aerosols, clouds, and radiative balance near Manus Island; 8) evaluate the effects of island topography on measurements of aerosols, clouds, and radiative balance; 9) examine details of the surface properties of the ocean and the dynamics of cool-skin and warm-layer effects (Fairall et al. 1996b); 10) obtain precipitation distributions and statistics in conjunction with simultaneous radar data; 11) investigate a host of remote sensor measurement and algorithm development issues; and 12) cross-calibrate measurements with similar DOE/CART instrumentation on Manus Island.

2. Cruise strategy and execution

Because of the importance of obtaining meaningful, simultaneous measurements with the ARM instrumentation at the TWP CART site, we needed to spend as much ship time as possible in the vicinity of Manus Island, Papua New Guinea. This required the *Discoverer* to steam at maximum speed from our starting point at Pago Pago, American Samoa (14.28°S, 170.68°W), to Manus Island (2.0°S, 147.3°E), and to then steam to our final destination of Honolulu, Hawaii (21.2°N, 157.8°W), at maximum speed. Rather than taking direct routes to these three ports, we decided to sacrifice a small amount of time and undertake a more meaningful survey of the central Pacific's warm pool by spending significant time cruising parallel to the equator between 1° and 2°S, a region relatively free of landmasses yet representative of equatorial conditions. We therefore planned a nominal track that progressed northwest from Samoa to 2°S, 180°W (date line), then directly west to a point northeast of the TWP CART site.

Although winds are highly variable in this part of the Pacific, a perusal of climatological winds prior to

the mission indicated that southwesterly flow is likely over Manus Island in March and April. An approach to the island from the northeast would permit the same airmasses to be sampled over Manus and by *Discoverer* and in the open ocean downwind of Manus, albeit not simultaneously. Therefore, we planned to steam southwest toward Manus Island until we were at a point 100 km from the island, and hold station for 2 days. We would then steam quickly to a point 30 km from the island and hold station for another 2 days before proceeding to the island and holding station there for 2 days. These stations would permit us, within synoptic-scale variability, to discern statistical differences in island-based and ship-based measurements as a function of separation, and thereby to begin to assess the representativeness of island-based measurements with respect to similar measurements over the open ocean.

Outbound from Manus to the northeast, we planned to reoccupy the same 30- and 100-km stations for another 2 days apiece, before repeating the meridional survey of the central Pacific by once again steaming east just south of the equator. This plan would carry us back to the point where we originally intercepted the 2°S parallel before diverting northeast to Hawaii. All significant data taking would therefore be space and time symmetric. Differences between measurements inbound to Manus Island and outbound would help quantify variability and representativeness in the region. The plan would give us 10 days in the vicinity of Manus Island, accomplish a 3200-km, 11-day survey of conditions in the west and central equatorial Pacific, and get the ship to Honolulu within our allotted mission time of 30 days.

The actual cruise track is shown in Fig. 1. To a large extent we were able to follow the nominal plan outlined above. However, while en route to Manus Island we were asked by NOAA to rescue one Tropical Atmosphere–Ocean (TAO) buoy that had broken loose from its mooring and was drifting near our track, and to service another nearby TAO buoy. We decided

to honor these requests, because the primary mission would not be compromised, and because the meridional survey would not be affected significantly. The only other important departure from the plan was the launch of a small, drifting heat-flux buoy from the first 100-km station. Instead of proceeding directly to the 30-km station 2 days later, we diverted the ship to recover the heat-flux buoy, which had been carried by currents to the west, considerably off our intended track. The Brookhaven National Laboratory (BNL) radiometer package was off-loaded at Manus Island when we arrived there on 27 March. It was subsequently installed and operated at the CART site for the remainder of the CSP mission.

3. Instrument descriptions and performance

Twelve organizations were involved in the mission:

- Colorado State University
- DOE/Brookhaven National Laboratory
- DOE/Los Alamos National Laboratory
- NASA
- Naval Postgraduate School

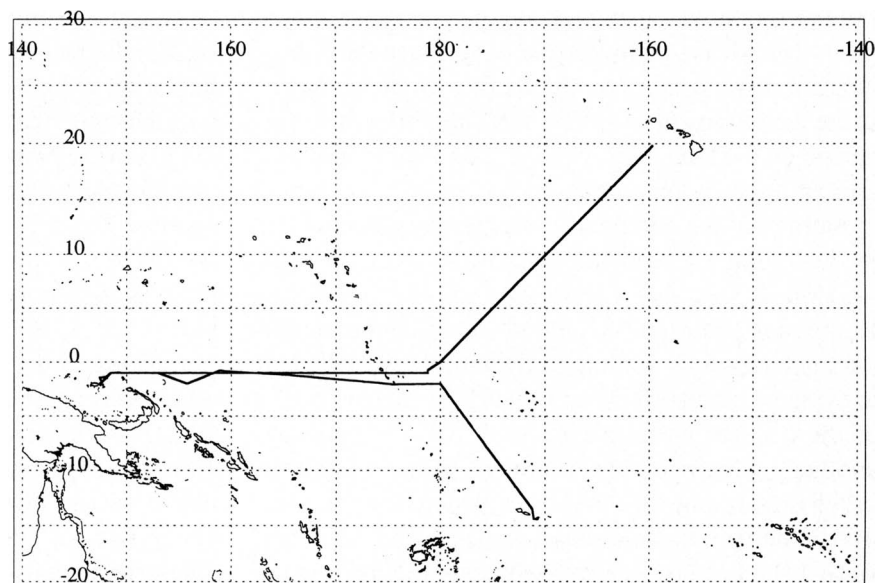


FIG. 1. Actual track of the CSP mission aboard the NOAA R/V *Discoverer* in the central and western Pacific, 14 March–13 April 1996. The mission began in Pago Pago, American Samoa (14.3°S, 170.7°W) and ended in Honolulu, Hawaii (21.2°N, 157.8°W). The westernmost point was just east of the DOE CART site at Momote, Manus Island, Papua New Guinea (2.0°S, 147.3°E).

- NOAA/Environmental Technology Laboratory
- NOAA/Pacific Marine Environment Laboratory (PMEL)
- The Pennsylvania State University
- University of Massachusetts
- University of Miami
- University of Washington
- University of Wisconsin

The instruments used during the mission are described below. Two of the instrument systems, the PMEL aerosol sensors and the NPGS AVHRR satellite receiver, had participated in prior FY96 *Discoverer* missions and had only to be reactivated and/or reconfigured to participate in CSP.

a. Radiosondes

Throughout the cruise we launched at least four balloons carrying Vaisala radiosondes per day, but near Manus Island we increased the frequency to eight per day. Both the ship's balloons and CSP balloons were launched, and often both the ship's receiver (A.I.R.) and CSP receiver (Cross-chained Loran Atmospheric Sounding System) tracked the sondes. Twice daily, for standard synoptic reporting times, sonde data were transmitted through the Geostationary Operational Environmental Satellite (GOES) into the Global Telecommunication System (GTS) database. In windy conditions (> 20 kt relative wind) launches were difficult and many sondes were lost, resulting in data gaps. Typical pressure altitudes reached by the sondes were 75 and 45 hPa for 100- and 200-g balloons, respectively.

There is some evidence that standard radiosondes may be subject to moisture biases in the Tropics. Systematic dry biases with Vaisala sondes on the order of 1 g kg^{-1} were observed in the boundary layer for groups of launches from a number of different platforms in TOGA COARE (Bradley and Weller 1997). Because of incomplete records, it is not known if this dry bias is associated with specific manufacturers, batches, or the handling of the sondes; some evidence suggests that storage in air-conditioned spaces just prior to launch may be a factor. For the CSP cruise, several steps were taken to minimize the thermal and humidity shock to which the sondes were subjected prior to launch. The sondes were stored in the shade at ambient temperature and humidity. During setup and the Omega navigation lock period (about 20–30 min), sondes were hung outdoors in a shaded space that was well ventilated with marine air. Sondes were

never allowed to bake in the direct sun prior to launch. A preliminary check of one sonde per day on 10 consecutive days yielded an average of 1.5 g kg^{-1} difference between the humidity at 20-m height (i.e., our surface observation) and a representative value for the mixed layer, close to the nominal difference of 1.25 g kg^{-1} expected on the basis of similarity theory and near-surface aircraft observations (Bradley and Weller 1997). Thus, our preliminary opinion is that dry biases were not a significant source of error for the CSP cruise; however, this issue will be examined in more detail. If there is a dry bias, it would cause a similar bias in radiometer retrievals of total integrated water vapor that were calibrated using radiosonde data. A bias of 1 g kg^{-1} over a depth of 1 km would represent a bias of about 0.1 cm, versus a typical total of 5 cm, in the amount of precipitable water vapor measured by the microwave radiometer.

b. Radar wind profiler

This mechanically stabilized 915-MHz system (Fairall et al. 1997) performed well, providing continuous coverage of horizontal and vertical components of wind in the lower atmosphere throughout the cruise. It often detected clouds and precipitation overhead. Its data acquisition parameters were matched to those of the Manus Island profiler, to facilitate comparisons. Lowest level winds (< 500 m) measured by this profiler may be contaminated by sea clutter, and may be biased low (up to 1 m s^{-1}).

c. Flux system

The high-speed (20 Hz) temperature, wind, and humidity sensors mounted on the bow tower worked well throughout the cruise, but the sensors' data-logging system experienced some startup problems during the first 3 days of the mission. The flux system sensed and compensated for instantaneous ship motion in real time. Broadband radiative fluxes and conventional bulk meteorological variables were also obtained as part of this system.

d. Cloud radar

This two-frequency, polarimetric system (Sekelsky and McIntosh 1996) experienced problems throughout the cruise, but through innovative repairs still acquired a significant dataset. It occupied a position far aft on the starboard fantail and was subjected to large-amplitude, low-frequency vibrations, especially when the ship accelerated. One of its air conditioners failed on the first day of the mission, necessitating replace-

ment. Only one frequency (95 GHz) was operative en route to Manus Island; the radar began taking data at 95 GHz the second day of the meridional survey (18 March). At Manus Island we received an emergency shipment of repair parts and got the 33-GHz channel working (28 March), but the 95-GHz channel failed nearly simultaneously. Thus, radar data obtained near Manus Island after 28 March and during the second (easterly) leg of the meridional survey were with the 33-GHz channel. However, on 7 April this channel became problematic again; hardware components and data taking were switched to the 95-GHz channel for the remainder of the cruise. Still, a significant new dataset for central and western Pacific clouds was obtained, especially when one considers simultaneously obtained supporting data. Images of cloud radar data are available at <http://abyss.ecs.umass.edu/CPRS-http/current>.

e. Marine-atmospheric emitted radiance interferometer (M-AERI)

This prototype instrument measured upwelling and downwelling infrared spectra at high spectral resolution (0.5 cm^{-1}) from near-visible to the thermal infrared wavenumbers ($550\text{--}3000\text{ cm}^{-1}$), both at zenith and at a number of nadir-viewing angles (Smith et al. 1996; Knuteson et al. 1997). This permits one to infer sea surface temperature of the top millimeter of the ocean (the “skin”) to a high degree of accuracy ($\pm 0.2\text{ K}$ absolute) and precision ($\pm 0.1\text{ K}$, 3 sigma), and to calculate profiles of atmospheric temperature and moisture in the marine boundary layer. It operated well throughout the cruise, acquiring good data 82% of the time. Periods of rain accounted for 12% of the downtime (optics were covered), while maintenance (2%) and loss of detector coolant (3%) accounted for most of the remaining downtime.

f. Fourier transform infrared radiometer (FTIR)

This instrument is similar to the M-AERI instrument, but it obtained data only while pointing vertically. Its resolution is 1.0 cm^{-1} with a spectral range from 500 to 2000 cm^{-1} (Shaw et al. 1995). This FTIR operated throughout the cruise, monitoring downwelling zenith radiation more continuously than the M-AERI did. During station keeping near Manus its blackbody references were realigned, after which time comparisons with the M-AERI were remarkably good. It is vital for proper analysis of FTIR and M-AERI data to know when clouds are overhead; information from the ceilometer, lidar, all-sky camera, microwave

radiometers, and cloud radar will therefore be used heavily in analyses of these data.

g. Microwave radiometers

This two-channel (23.87- and 31.65-GHz), zenith-viewing system continuously and simultaneously monitored integrated cloud liquid and gaseous water substance overhead. The system employed a spinning reflector (Jacobson and Nunnelee 1997) to direct downwelling radiation from the atmosphere into the radiometers’ antenna and prevent accumulation of precipitation, thus permitting observations in nearly all weather conditions. Satisfactory tip-calibrations (Hogg et al. 1983) were not possible due to a small antenna misalignment that could not be corrected under way, because of ship motion. Instead, data from 19 radiosonde profiles acquired under clear conditions during the early part of the mission were used to calibrate the system, which performed continuously and solidly throughout the mission. Any bias in radiosonde-derived integrated water vapor will cause a bias of similar magnitude in the radiometer data (see discussion on biases in section 3a above).

h. Elastic and Raman lidar

Two lidar systems were used during the mission—a solid-state Nd:YAG system that produces pulses of light at $1.06\text{ }\mu\text{m}$ (near infrared) and $0.53\text{ }\mu\text{m}$ (green), and an excimer gas (fluorine) system that produces pulses of light at $0.24\text{ }\mu\text{m}$ (ultraviolet). The former system measures light backscattered from aerosols, cloud particles, and air molecules, which is nearly unchanged in frequency, except for possible Doppler shifts; hence, it is called an elastic lidar. The ultraviolet lidar measures weak signals that have been reemitted by lidar-excited molecules at a frequency typically below the exciting frequency. The amount of the shift represents the vibrational or rotational state to which the molecule was excited, as discovered by Raman; the amount of shift is species specific, enabling one to measure the concentrations of different gaseous components of the atmosphere. By measuring the amount of Raman-shifted light from both water vapor and nitrogen molecules as a function of range, the Raman lidar can remotely measure the mixing ratio profiles. By scanning the lidar beam, one can map areal or vertical distributions of the gasses (Cooper et al. 1997).

Both lidars began collecting data the second night of the mission (16 March), including a series of moisture and aerosol profiles up to cloud-base level, and

at times higher. However, within 8 h it was discovered that smoke, oil, and soot from the ship's engine exhaust had deposited on the lidars' scanning mirrors. When these deposits were illuminated by the intense laser light, they vaporized, oxidizing the mirrors' coatings as well. The result was nearly disastrous (total loss of both lidars), but the lidar operators developed ingenious temporary solutions to allow partial data taking. Even with frequent cleaning of the remaining optics, all exposed mirrors were completely ruined by 3 April. About this same time the high-voltage supply for the Nd:YAG laser failed irreparably. The combination of events curtailed all lidar data acquisition for the remainder of the mission (10 days). Despite the setbacks, exciting new results were apparent in the data, and the lidar observations will be vital for interpreting several of the other datasets (e.g., from the M-AERI, FTIR, and aerosol samplers).

i. Ceilometer

This small, eyesafe, commercial laser radar system performed continuously throughout the cruise, measuring cloud bases occurring below 3.66 km (12 000 ft) altitude. A similar instrument on Manus Island was set up to record cloud bases to higher altitudes of 7.62 km (25 000 ft).

j. AVHRR and GMS satellite sensors

Except for 23 and 24 March, when the satellite receiving system had to be realigned after a computer power failure, AVHRR satellite data were received continuously throughout the mission. Images of 1.1-km resolution were obtained in five channels of wavelength 0.63, 0.86, 3.7, 11.0, and 12.0 μm . Geostationary Meteorological Satellite (GMS) water vapor images of 0.1° (62 km) resolution in the 6.5–7.0- μm band were also archived for postanalysis. Degraded images of 0.25° (156 km) resolution were made into video "loops" in S-VHS format, with each loop showing synoptic-scale features and the ship's track. The higher-resolution GMS images are available at <http://www.cdc.noaa.gov/climsat/products.html>.

k. Aerosol samplers

The in situ samplers for characterizing boundary layer aerosols performed admirably throughout the cruise. Both aerosol chemistry and size distribution were measured continuously and results were plotted in near-real time throughout the cruise (Quinn et al. 1996). Sample air for all measurements was drawn through a 6-m-long heated sample inlet and dried to

50% relative humidity. The top of the inlet was 18 m above sea level and 10 m forward of the ship's stack. Measurements were made only when the concentration of particles > 15 nm diameter was small enough to indicate no contamination, the relative wind was > 3 m s⁻¹, and the relative wind direction was forward of the inlet.

The number size distribution between 0.02 and 0.6 μm was measured every 10 min with a differential mobility particle sizer at a relative humidity of 30%. The number density between 0.6 and 9.6 μm was measured at the same time at a relative humidity of 50% by an aerodynamic particle sizer. Seven-stage multijet cascade impactors were used to determine mass size distributions of Cl⁻, Br⁻, NO₃⁻, SO₄⁼, MSA⁻, Na⁺, NH₄⁺, K⁺, Mg₂⁺, and Ca₂⁺, with time resolution of 12–24 h. For these measurements, the 50% aerodynamic cutoff diameters were 0.27, 0.37, 0.64, 1.2, 2.3, 4.7, and 12.0 μm . Two-stage impactors measured total organic and elemental carbon on a 3-day timescale. Aerosol total scattering and hemispheric backscattering coefficients were determined with an integrating nephelometer at wavelengths of 0.45, 0.55, and 0.70 μm . The aerosol absorption coefficient at a wavelength of 0.55 μm was also measured. Interpretation of these detailed aerosol size and chemistry data give strong indications of surface air mass origin and age, and they will be valuable in better understanding sea–air–cloud interactions and the shortwave radiative balance.

l. SST sensors

A number of in situ and remote sensors measured the skin, surface, and bulk temperatures of the upper ocean throughout the cruise. These included the ship's measurements on water drawn from a depth of 5 m near the bow, two infrared thermometers, two floating sensors, and M-AERI. The floating sensors were deployed only while the ship was holding station or moving slowly. The complete set of readings permits us to quantify and understand relationships between SSTs measured at depths of 1 mm, 10 cm, and 5 m.

While the ship was station keeping, it was pointed approximately into the wind with sufficient power to maintain about 1 m s⁻¹ forward motion. This allowed us to maintain steerage and to minimize any potential thermal effects of the ship's hull on the near-surface sea temperature measurements. Both near-surface sea temperature sensors were trailed in the water from outrigger booms near the bow to keep them 2–3 m away from the hull. Turbulence shed from the ship's hull may have generated some local vertical mixing,

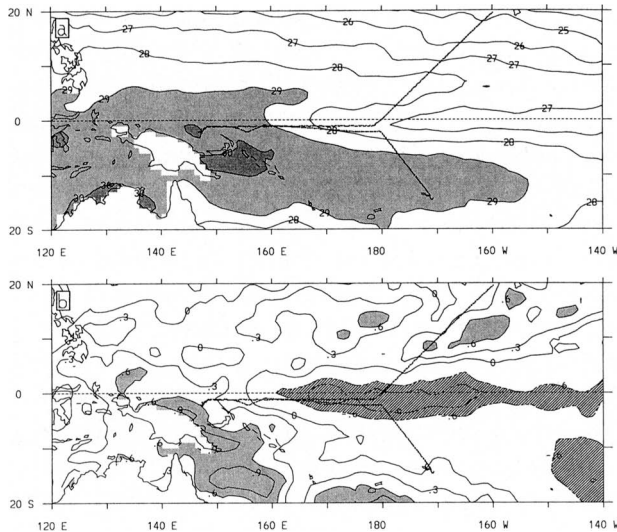


FIG. 2. The time-mean sea surface temperature for 15 March–15 April 1996: (a) total SST field displayed with a contour interval of 1°C and with values > 29°C shaded; (b) anomalous SST field displayed with a contour interval of 0.3°C and with negative contours dashed; values $\geq 0.6^\circ\text{C}$ ($\leq -0.6^\circ\text{C}$) are shaded (hatched). The line segments show the *Discoverer* ship track during the CSP; they are also shown on the three subsequent figures.

but this modest forward speed should have been sufficient to eliminate significant warming of the water at the sensors.

m. All-sky camera

This system began recording hemispherical images of the sky and clouds shortly after we began the first (westward) half of the meridional survey, but only during daylight hours. On the second (eastward) half of the survey it also recorded images at night when there was sufficient moonlight. Time-lapse animation of the entire mission's image sequence is available in VHS format.

n. Sun photometer

This multichannel (filter wheel) instrument was on its first field deployment and experienced considerable problems. It acquired direct solar flux data at several visible and infrared wavelengths intermittently before *Discoverer* arrived at Manus Island, but only when it was pointed and held on the sun manually. During station keeping near Manus Island it began to track the sun automatically, but not reliably. Therefore, more data were acquired during the second half of the mission, but they must be scrutinized for accuracy, as misalignments can easily be misinterpreted as increased atmospheric attenuation.

o. Portable radiation package

This system of several radiometers performed nearly flawlessly during the first half of the mission, providing important information on direct and diffuse solar (shortwave) radiation, and downwelling infrared radiation (Reynolds and Smith 1997). For the last half of the CSP mission it was taken off the ship, then set up and operated on Manus Island, where it performed equally well.

p. Rain sensors

Two STI optical rain gauges (Sheppard and Joe 1994; Wang et al. 1978) measured rainfall rates on both sides of the ship. The sensor on the windward side appeared to provide better readings than the one on the leeward side. Rain rates up to 142 mm h^{-1} were recorded. Disdrometers measured the raindrop size spectrum and appeared to perform well throughout the cruise. However, after the cruise, serious concerns about calibration and linearity raised doubts that any of the rain data can be used quantitatively.

q. Surface meteorological sensors

In addition to the ship's meteorological sensors for surface air temperature, humidity, and pressure (approximately 33, 12, and 10 m above sea level, respectively), there were several other independent sets of sensors measuring the same variables. Spot intercomparisons were not always satisfying. Handheld standards for temperature and relative humidity were taken to each sensor, and readings were taken simultaneously to help remove biases when data are postprocessed.

r. Heat flux buoy

A small drifting-buoy system (Soumi et al. 1996) was deployed when *Discoverer* arrived northeast of Manus Island at the first 100-km station. A floating sensor for measuring surface heat flux was tethered to it. The buoy regularly transmitted its position and sensor data to the University of Wisconsin via the ARGOS satellite. This experimental system was retrieved 2 days later en route to the first 30-km station, but it was not deployed again because the sensor was faulty. However, some reliable data were obtained by the system.

4. Meteorological context

An important postcruise activity was to review and summarize the meteorological conditions throughout

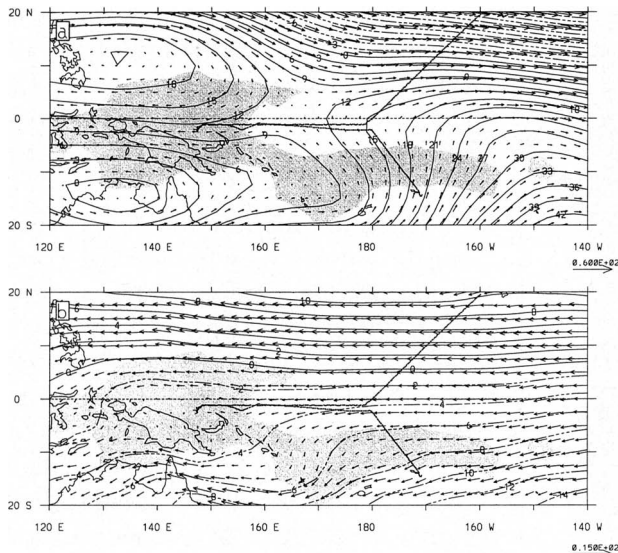


FIG. 3. The time-mean streamfunction field ψ and nondivergent wind field for 15 March–15 April 1996 at (a) the 150-hPa level and (b) the surface. The contour interval in (a) is $3 \times 10^6 \text{ m}^2 \text{ s}^{-1}$ and in (b) is $2 \times 10^6 \text{ m}^2 \text{ s}^{-1}$; negative contours are dashed. The wind vectors are linearly scaled relative to the arrows shown at the lower right. Units are m s^{-1} . The total vector wind field is given by the sum of the nondivergent and divergent winds (see Fig. 4). Shading shows regions where OLR is $\leq 230 \text{ W m}^{-2}$.

the cruise and to compare them with mean conditions for the month. An in-depth report, summarized below, was produced and distributed to principal investigators (PIs). Mean conditions were derived from reanalysis of an historical 40-yr dataset (Kalnay et al. 1996). Knowledge of the synoptic and regional meteorology is needed to better interpret and analyze the data.

Three phenomena provide insight into the time-mean and time-varying large-scale atmospheric circulation observed during the CSP. Two of these, the annual cycle and El Niño–Southern Oscillation (ENSO), helped determine the time-mean CSP conditions, while the third, Madden–Julian oscillations (Madden and Julian 1972), dominated the large-scale time-varying part. As is typical for the coupled ocean–atmosphere system (Bjerknes et al. 1969; Graham and Barnett 1987), we experienced a close relationship between the pattern of SST and tropical convection. The occurrence of large-scale, deep convection increased substantially as the ship moved into waters having temperatures $> 28^\circ\text{C}$. To a good approximation, the atmospheric circulation could be understood as a response to the divergent flow associated with this convection (Gill 1980).

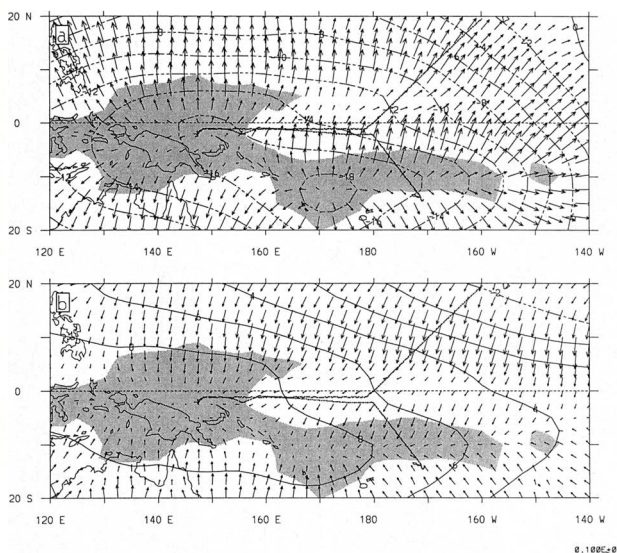


FIG. 4. The time-mean velocity potential field χ for 15 March–15 April 1996 at (a) the 150-hPa level and (b) the surface. The contour interval is $2 \times 10^6 \text{ m}^2 \text{ s}^{-1}$; negative contours are dashed. Divergent wind vectors are superimposed; the arrow scaling is shown at lower right. Shading shows regions where OLR is $\leq 230 \text{ W m}^{-2}$.

The time-mean SST and its departure from a 15-yr climatology are shown in Figs. 2a and 2b, respectively. Normally during northern spring the center of the west Pacific Ocean warm pool is in the Southern Hemisphere (Fig. 2a), and equatorial SST gradients are weak in the region traversed by the *Discoverer*. In a typical year, convection occasionally reaches eastward to the date line, the equatorial cold tongue is weak, and SSTs approach 28°C there. This tendency was disrupted during the CSP by a weak to moderate cold event within the ENSO cycle, which moved equatorial convection to regions west of 160°E . The observed SST anomalies (Fig. 2b) produced a stronger zonal SST gradient along the equator, with 27°C water at the date line becoming 29°C water at 160°E . As a result, strong gradients in convective activity and in the atmospheric zonal circulation were also located near 160°E .

The time-mean atmospheric wind field, decomposed into streamfunction ψ and velocity potential χ fields, is shown in Figs. 3 and 4, respectively. The ψ and χ fields depict the nondivergent (Fig. 3) and divergent (Fig. 4) components of the flow. The two levels shown in each figure were chosen to be near the layers of maximum inflow (surface) and outflow (150 hPa or 15 km) associated with deep tropical convection. In both figures, the pattern of deep convection is illustrated by shading of outgoing longwave

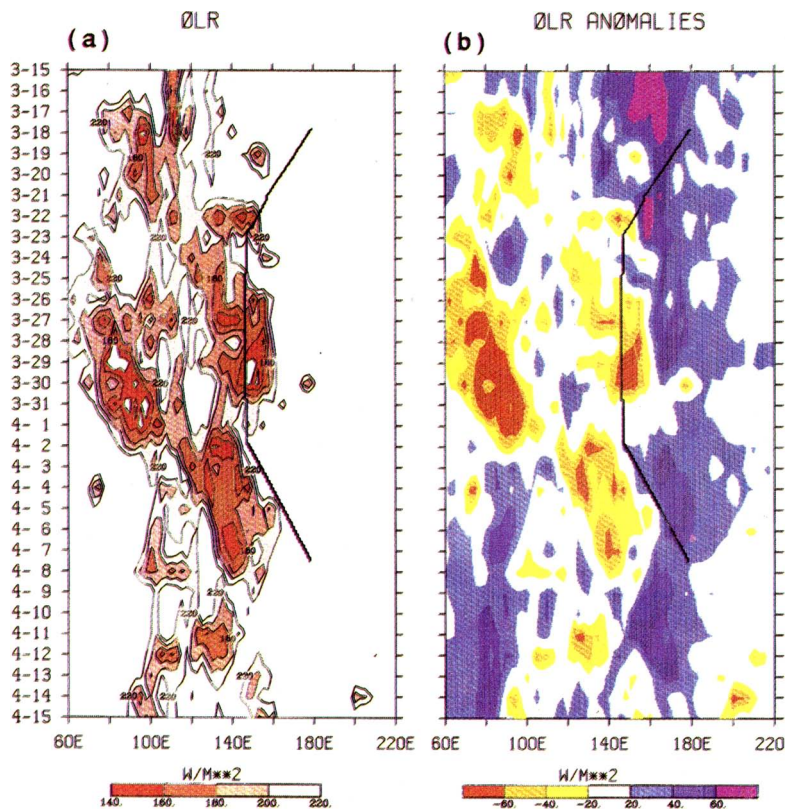


FIG. 5. A longitude–time plot of daily mean OLR averaged between 0° and 2.5°S for the CSP period: (a) total OLR with a contour interval of 20 W m^{-2} and the shading table shown below; (b) anomalous OLR with the shading table shown below. The ship track is shown with a heavy black line.

radiation (OLR) values $< 230\text{ W m}^{-2}$. OLR is frequently used as a proxy for deep tropical convection (Waliser et al. 1993).

The 150-hPa ψ field (Fig. 3a) shows a pattern of stationary waves consisting of twin anticyclones straddling the equator along 130°E and cyclones on either side of the equator centered well east of the date line. Along the equator easterly flow between the two anticyclones becomes westerly flow east of $\sim 165^{\circ}\text{E}$. The surface ψ field (Fig. 3b) shows the general easterly trade wind flow giving way to weak cyclonic features in the western Pacific beneath the upper-level anticyclones. Equatorial convection is located in the upper-level easterly flow between the twin anticyclones and in weak westerly flow at the surface. The Fig. 4 χ fields show upper-level divergence and low-level convergence in the regions of time-mean deep convection (shading), especially over the western Pacific Ocean. Axes of 150-hPa divergence and surface convergence then extend eastward in two convergence zones on either side of the equator. These are approximately coincident with a similar structure in the time-mean

convective pattern, which, however, is more intense in the Southern Hemisphere. Enhanced subsidence occurs along the equator between the two convergence zones in the region of cooler than normal SST.

The time-mean conditions were largely controlled by ENSO cold-event conditions that spread westward from the east Pacific in spring 1995 reaching the west Pacific during spring 1996. The other large-scale phenomenon controlling convection in and to the east of the warm-pool region is the so-called Madden–Julian oscillation (Madden and Julian 1972). The MJO is characterized by large-scale convective flareups that develop over the Indian Ocean and then move east to the Pacific Ocean (Lau and Chan 1985; Knutson and Weickmann 1987). Individual MJOs represent the convective envelope for a wide range of convective activity that evolves and decays on many time and space scales (Nakazawa 1988; Hendon and Liebmann 1994). For daily-mean data, the most prominent of these multiscale features is the so-called supercluster that seems especially well-defined in the spring and

fall seasons when the seasonal-mean convective activity occurs near the equator.

A detailed picture of the time evolution of deep convection during the CSP can be seen in the time–longitude diagram in Fig. 5. Both the total (Fig. 5a) and anomalous (Fig. 5b) OLR depict the MJO that affected the western Pacific region during the CSP mission (late March to early April 1996). The MJO consisted of two superclusters both of which developed over the Indian Ocean and then moved eastward at a speed of $\sim 8\text{ m s}^{-1}$. The first supercluster reached the area of Manus Island while the *Discoverer* was on station and gave the most intense and prolonged convection experienced during the cruise (at least in equatorial regions). The second supercluster was somewhat stronger, but its convection set up slightly farther to the west ($\sim 140^{\circ}\text{E}$) as the ship left Manus Island. However, as a result of this convective development, the atmospheric circulation in the cold-tongue region during the *Discoverer*'s eastward return journey in early April had changed compared with the westward track in mid-March, especially in upper levels.

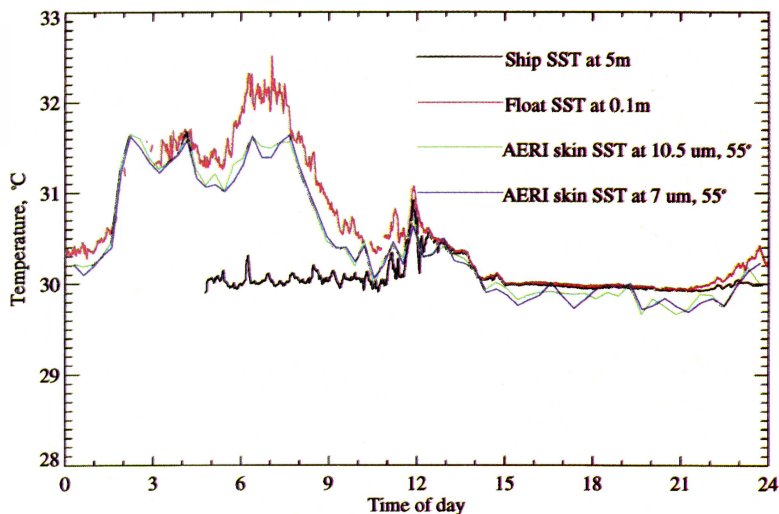


FIG. 6. Diurnal cycle of SST at depths of 5, 0.1, and 0.001 m (“skin”) under calm conditions at the first 30-km station (1.84°S, 147.65°E), 24 March 1996. Time is UTC. Local noon is approximately 0210 UTC.

In summary, the atmospheric circulation over the western and central equatorial Pacific during spring 1996 was somewhat atypical; it had stronger than usual zonal gradients in SST, convection, and atmospheric zonal winds. These features primarily reflected a weak to moderate cold event in the ENSO cycle. Although the center of persistent, large-scale convection was confined to the far western Pacific Ocean region, a Madden–Julian oscillation and its associated synoptic variability provided an episode of deep convection somewhat farther east over Manus Island while the *Discoverer* was on station.

5. Preliminary results

About 6 months after the mission, on 28–29 October 1996, the CSP science team held a workshop in Boulder, Colorado, to examine preliminary data. Prior to the workshop, many datasets were contributed to a web-accessible data management system at ETL, and more datasets have been contributed subsequently. The team decided to password-protect CSP datasets until PIs ensured their quality, had the first chance to use them, and published findings. The data management system makes it convenient to access others’ data in a common format (netCDF) and to use datasets synergistically. These data are

available to the entire DOE/ARM community; soon the public will have access. CSP and Manus Island datasets that have been contributed to ETL’s data management system are listed in Table 1. Several PIs have created Graphics Interchange Format (GIF) images of their data and made them available via the World Wide Web. Visit <http://www4.etl.noaa.gov> to learn about both data and image sites. What follows in this section is a pot-pourri of glimpses at CSP data.

Among the immediate payoffs of combining and comparing datasets was a better understanding of interrelationships between various types of SST measurements. Figure 6 depicts a 24-h period at the initial 30-km station northeast of Manus Island, when winds were calm or light. During daylight hours SST in the upper layer of the sea (0–5 m) increases due to insolation, but relatively large temperature differences occur between the ship’s sensors sampling water at a depth of approximately 5 m, other sensors at 0.1-m depth, and the M-AERI instrument, which measures the temperature of the radiating skin, which is nominally 1-mm deep. The skin temperature is generally a few tenths of a kelvin lower than the temperature of the water immediately below it, due to evaporative cooling. Surface layer overturning in the absence of insolation at night tends to equalize all three measurements. Combined

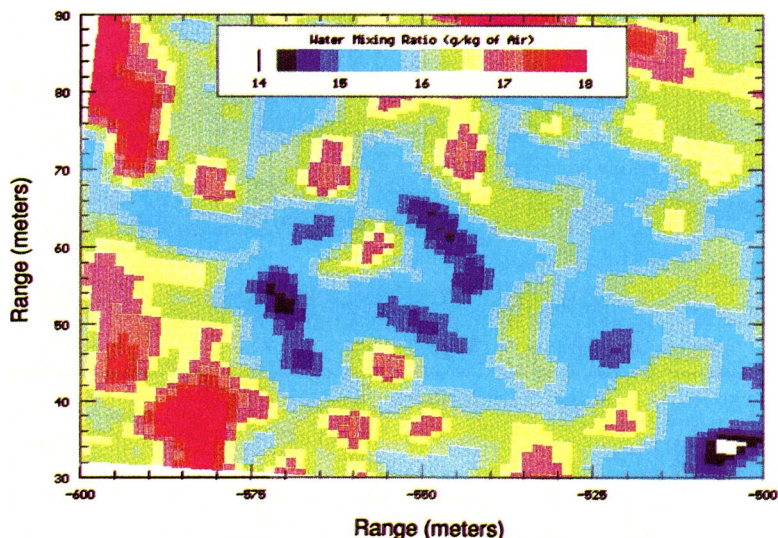


FIG. 7. Horizontal scan of the Raman lidar a few meters above the sea surface, revealing an organized pattern of water vapor cells with dimensions of the order of 10 m, 26 March 1996.

TABLE 1. CSP and Manus Island datasets (in ETL Data Management System).

CSP	Manus Island
Aerosol size distributions	Pyranometer flux
Aethalometer absorption	915-MHz winds (moments) w/RASS*
Anemometer relative wind (1-min avg)	915-MHz winds (spectra) w/RASS
Anemometer relative wind (30-min avg)	Rotating shadowband radiometer
Anemometer wind (30-min avg)	Surface meteorology
Rawinsonde (CLASS)	Pyrgeometer
Ceilometer	Ceilometer
Fluxes, meteorological	
FTIR spectra	
MAERI spectra	
Nephelometer, submicrometer	
Nephelometer, total	
Rain Rates, optical (CSU/NASA)	
Meteorology, PMEL	
Rain rates, optical (PMEL)	
Radon	
Pyranometer flux (BNL)	
Pyranometer flux (PMEL)	
Pyranometer flux (ETL)	
915-MHz winds (moments)	
915-MHz winds (spectra)	
Water vapor and liquid (microwave radiometer)	
Rotating shadowband radiometer	
Seawater chemistry	
Ship's meteorology and ocean data	
Ship's navigation data	
Observers' meteorological notes	

*with Radio Acoustic Sounding System

measurements such as these help better understand the radiation budget and air–sea interactions (Webster et al. 1996; Soloviev and Schlussel 1996; Fairall et al. 1996b).

Under these same calm conditions the Raman lidar detected a pattern of water vapor cells that were

tens of meters in diameter (Fig. 7), a pattern never before seen or hypothesized (Cooper et al. 1997). This discovery can be corroborated by statistical intercomparisons with data from other CSP sensors, such as radiometers, flux systems, and the wind profiler, possibly leading to a better understanding of moisture flux at the surface. These finescale observations will help us better understand the mechanics by which moisture and latent heat are carried aloft from the sea surface under nearly calm conditions.

Figure 8 depicts the time histories of both integrated water vapor (red) and integrated liquid water in clouds (blue) for the periods of station keeping near Manus Island, at 100 km (top two panels), 30 km (third and fourth panels from the top), and close to the island (bottom panel). Downward-pointing arrows indicate that rain was detected at the surface. These data corroborate other data (e.g., ceilometer data) that indicate it was relatively dry and less cloudy far removed from the island (100 km stations) than at the 30 km or nearby stations. Whether or not this is a general trend or one induced by transient synoptic meteorology remains to be determined by further inspection of the meteorological analyses mentioned in the previous section.

Figure 9 depicts the radiance difference between two independently operated FTIRs, one from NOAA/ETL and the other from the University of Wisconsin. Absolute radiances for both instruments were in the range 40–100 $\text{mw m}^{-2} \text{sr}^{-1} \text{cm}$ for the 700–1300 cm^{-1} band. The rms difference shown in Fig. 9 is well below 1 $\text{mw m}^{-2} \text{sr}^{-1} \text{cm}$ and is very small on a relative basis. This is a typical comparison, and it corroborates the empirical adjustment to an ARM-standard, line-by-line radiative transfer model (LBLRTM) made by S. Clough, based

on ETL FTIR spectra taken during TOGA COARE and CSP (Shaw et al. 1995; Han et al. 1997). Figure 10 shows the radiance differences between the model and measurements (a) before and (b) after the adjustment. The Air Force Geophysical Laboratory (AFGL)

subsequently adopted this adjustment for LOWTRAN, MODTRAN, and FASCOD, improving these highly used algorithms. Accurate high-resolution FTIR measurements such as these can be used to retrieve profiles of temperature and atmospheric constituents in the boundary layer, thereby more thoroughly characterizing it, and to measure SST. Of course, by scanning from nadir to zenith they also provided a very detailed assessment of infrared upwelling and downwelling flux at the surface to better understand radiative balance. For these devices it is critical to know when clouds are in the field of view because clouds are strong infrared radiators. Therefore, simultaneous measurements by the microwave radiometer, cloud radar, ceilometer, lidar, all-sky camera, and other CSP sensors help considerably in data analysis.

The measured aerosol number size distribution as a function of meteorological regime is shown in Fig. 11. Within the South Pacific convergence zone (SPCZ) and the intertropical convergence zone (ITCZ) deep tropical cumuliform clouds persist and precipitation occurs frequently; here the Aitken mode (particle diameters between 20 and 70 nm) dominated the size distribution. Sporadically an ultrafine mode (diameters < 20 nm) appears, possibly transported by air from the upper troposphere into the boundary layer by subsidence. There was no detectable accumulation mode (diameters between 70 and 500 nm) because of aerosol scavenging by precipitation. In the wedge-shaped region between the SPCZ and ITCZ divergent easterly winds prevailed and precipitation was much less frequent. Here the size distribution is distinctly bimodal, showing both Aitken and accumulation modes. Near Manus Island, three

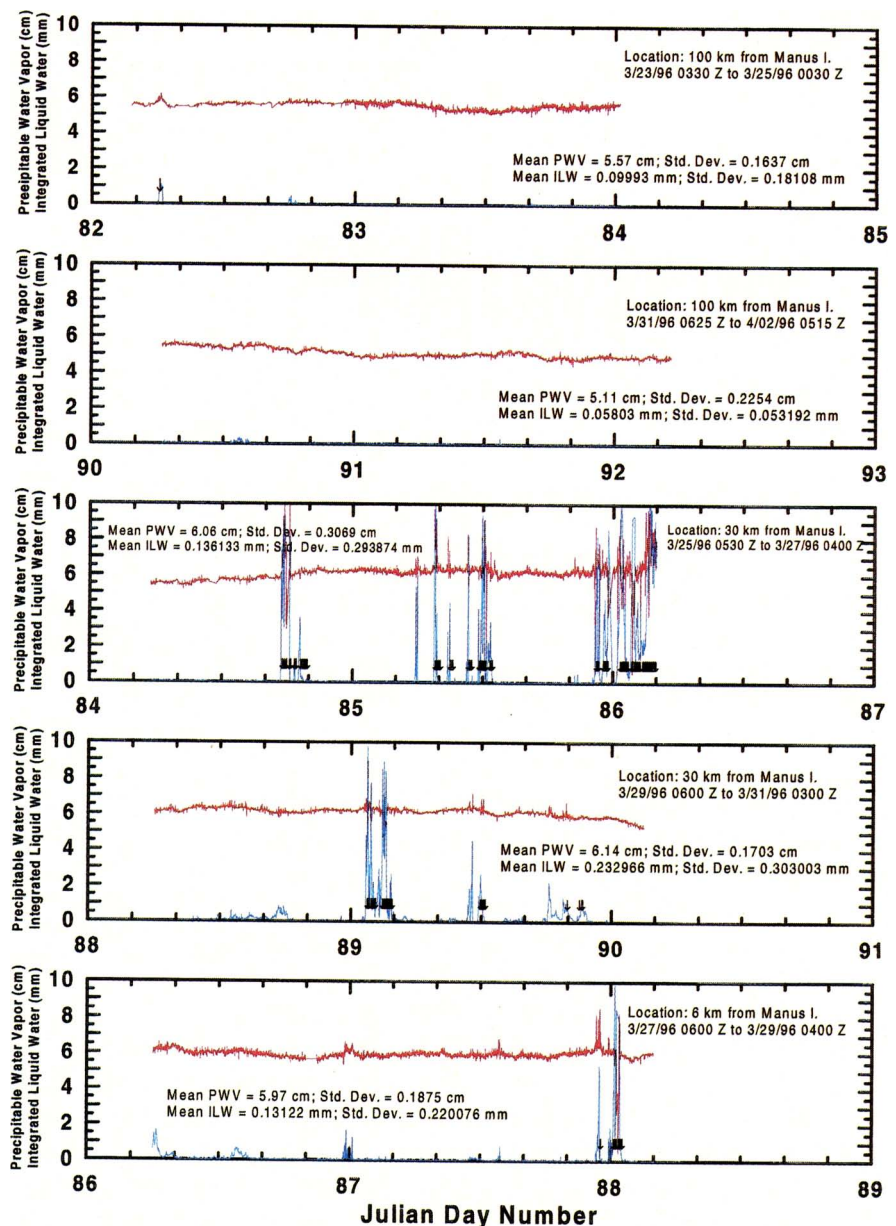


FIG. 8. Time histories of precipitable water vapor (red) and integrated liquid water (blue) for periods of station keeping near Manus Island, derived from microwave radiometer data. The top two panels are for the 100-km station, the third and fourth panels are for the 30-km station, and the bottom panel is for the station closest to Manus Island. Downward-pointing arrows indicate times for which precipitation was detected at the surface.

meteorological situations were encountered over the 10-day period. During “Manus dry” and “Manus wet” the accumulation mode was depleted, again indicative of an air mass scavenged by precipitation. During “Manus old” the size distribution was bimodal, indicating less frequent precipitation. Here a larger mean diameter of Aitken particles implies that the aerosol is well aged and may have been transported from the region of divergent easterlies. Inbound to Hawaii we

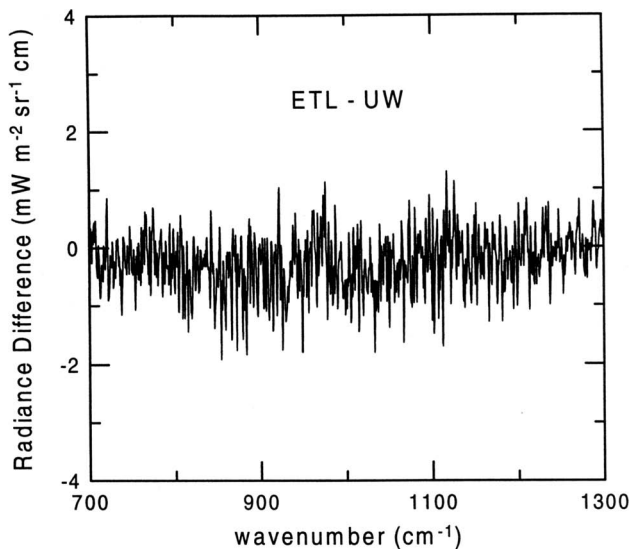


FIG. 9. Difference of simultaneously measured radiances between the University of Wisconsin and ETL high spectral-resolution FTIR instruments, showing remarkable absolute agreement across the 700–1300 cm^{-1} band, 0804 UTC 2 April 1996.

experienced northeast trade winds and size distributions similar to those found in the divergent easterlies. However, the air mass here appears to have been more anthropogenically influenced because the concentration of elemental carbon, which results from combustion, was higher. Also, the concentration of radon, which serves as a tracer for continentally derived air, was higher. See Quinn et al. (1996) for common features between this CSP summary and data from earlier RITS and ACE campaigns in the Pacific.

Comparisons between the ceilometer onboard *Discoverer*, a device with a maximum altitude extent of 3.66 km (12 000 ft), and the ceilometer at the Manus Island CART site, a 7.62-km (25 000 ft) device, were revealing. Table 2 summarizes the cloud-fraction and cloud-base statistics as functions of platform (ship or island) and ship location (by zone). It also shows correlation statistics between ship- and island-based ceilometers. As expected, correlation decreases with increasing separation, but is still significant at 30-km separation. Figure 12 depicts the detailed track of the ship for the 10 days it was within 100 km of the island, and shows the three zones cited in Table 2 associated with station keeping.

Figure 13 indicates that the cloud fraction over the island was always higher than over the ship, even if the island ceilometer data were processed only to the same altitude as the ship's data (3.66 km). The island ceilometer detected clouds above 3.66-km altitude that

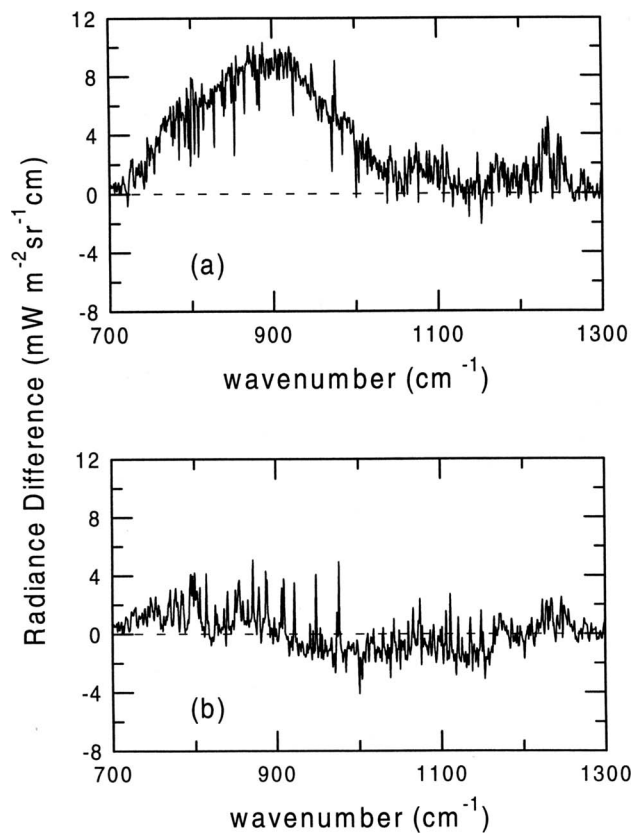


FIG. 10. Differences between modeled and observed radiance before (a) and after (b) an adjustment was made to the model by AFGL, based on TOGA COARE measurements in 1995.

increased in the late afternoon, persisted through the evening, and finally dissipated in the early morning hours. These midlevel clouds may have been the result or remnants of daytime convective activity over mainland Papua New Guinea. Probability distributions for the bases of low clouds (< 3.66 km) over both the ship and island were quite similar, as shown by Fig. 14. Such ceilometer data, when compared to appropriately averaged radiative flux and SST measurements, will help assess the effect of clouds and cloud base on these variables.

Figure 15 shows a 24-h segment of simultaneously acquired reflectivities from radars at three different frequencies: (a) 915-MHz wind profiler on *Discoverer*, (b) 3-GHz precipitation radar on Manus Island (Ecklund et al. 1995), and (c) 33-GHz cloud radar on *Discoverer*. The UTC date is 30 March 1996. Data were acquired while *Discoverer* was at the 30-km station, downwind from Manus Island. Thus, precipitation events in the middle panel (Manus Island data) appear slightly earlier than corresponding events in the top and bottom panels (*Discoverer* data).

Relationships between the reflectivities seen in these panels can be used to determine microphysical properties of the clouds and precipitation, such as rain rate, size distributions, effective radii, etc., important quantities for modelers of clouds, precipitation, boundary layer processes, and radiative balance.

6. Summary

The CSP mission brought together and operated a unique combination of shipborne in situ and remote sensors in the central and western equatorial Pacific ocean for a 30-day period beginning 14 March 1996. The combination of sensors characterized the marine boundary layer, the radiation budget, air–sea interactions, and clouds more completely than did any previous campaign. The unique combinations of measurements should lead to better understanding of fundamental climate-related processes and feedbacks, interferences to satellite data products, and the representativeness of CART measurements on Manus Island.

The operations plan for CSP was executed nearly flawlessly, and all major goals of the mission were accomplished. The CSP dataset has already resulted in new insights to fundamental processes important to the modeling of climate (e.g., see discussion in section 5), and more are anticipated. The SST measurements, and their interrelationships under a variety of meteorological conditions, will be used to improve

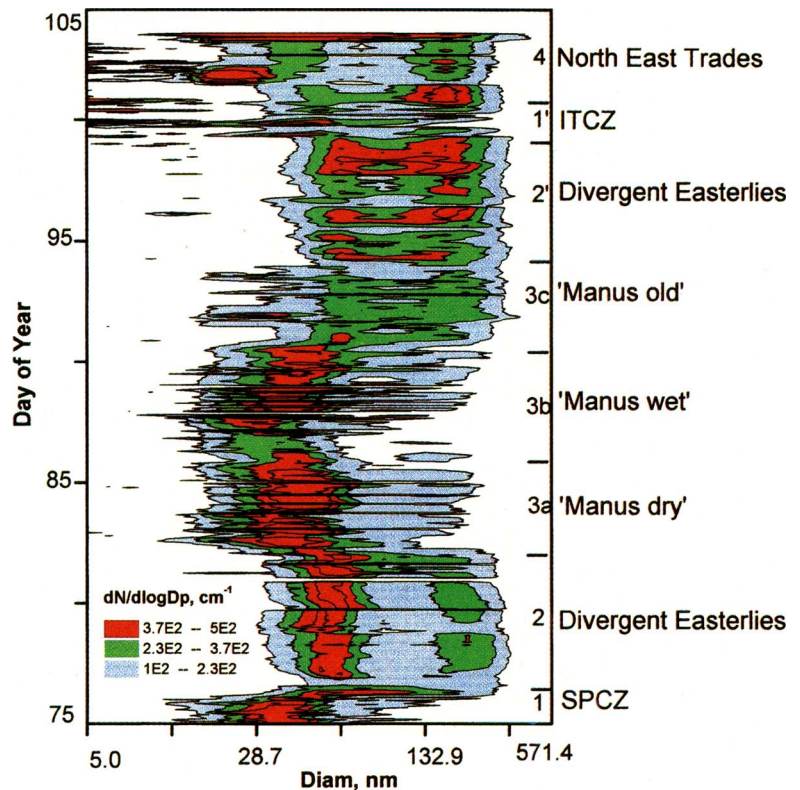


FIG. 11. Contour plot of surface aerosol size distribution changes throughout the CSP mission, with hypothesized airmass types indicated.

satellite SST retrievals and better understand and parameterize energy and moisture fluxes across the air–sea interface. Other investigations remain. For example, enhancements in aerosol backscatter just below cloud base can be compared with lifting/growth models to verify the models and the assumption of a well-mixed marine boundary layer. On the eastbound return leg we unexpectedly experienced small regions of dry downwelling air, where ozone and the concen-

TABLE 2. Statistics from data collected by a ceilometer on board *Discoverer* in zones 1–3 (Fig. 12) and by a ceilometer at the Manus Island CART site. Here N_{cf} is the number of data points in cloud-fraction correlation; r_{cf} is the cloud-fraction correlation coefficient; N_{ch} is the number of data points in cloud-base height correlation (restricted to cloud fractions > 0.1 for hourly data and cloud fractions > 0.5 for 10-min data); and r_{ch} is the cloud-base height correlation coefficient.

Ship location	Cloud fraction		Median cloud-base height (m)		Hourly data				10-min data			
	Island	Ship	Island	Ship	N_{cf}	r_{cf}	N_{ch}	r_{ch}	N_{cf}	r_{cf}	N_{ch}	r_{ch}
Zone 1	0.28	0.08	960	732	55	0.08	13	−0.29	342	−0.01	77	0.15
Zone 2	0.34	0.24	1065	1128	90	0.69	43	0.38	526	0.56	195	0.35
Zone 3	0.19	0.12	1455	1471	42	0.84	11	0.95	250	0.67	47	0.62

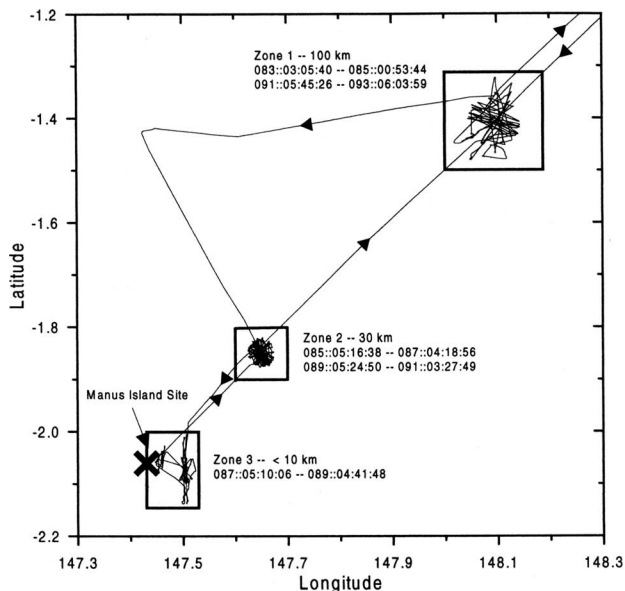


FIG. 12. Detailed track of *Discoverer* near Manus Island, Papua New Guinea. Zones 1, 2, and 3 were the nominal 100-, 30-, and 0-km stations, occupied a total of 4, 4, and 2 days, respectively. The Julian days and times in the zones are shown.

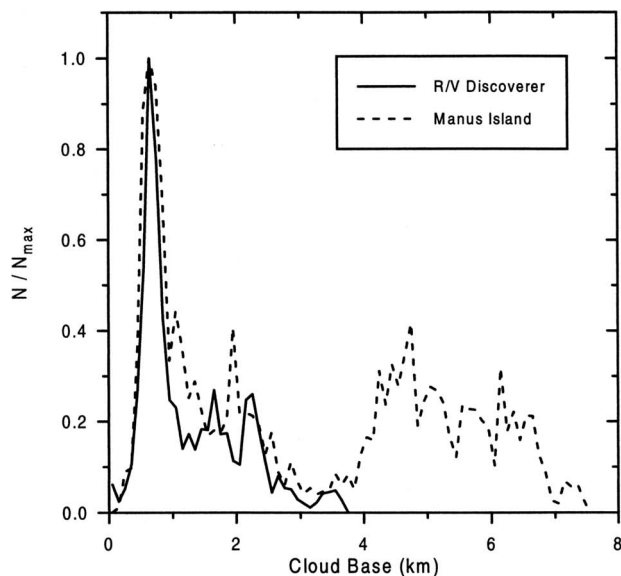


FIG. 14. Probability distribution of cloud bases measured by the ship's ceilometer (solid) and the island ceilometer (dashed), for the 10-day period while the ship was within 100 km of Manus Island. The ship's ceilometer acquired data to an altitude of 3.66 km, while the island ceilometer acquired data to an altitude of 7.62 km.

tration of small (new) particles rose dramatically. These regions may have been on the boundary between different air masses and may be important in the downward mixing of important species generated

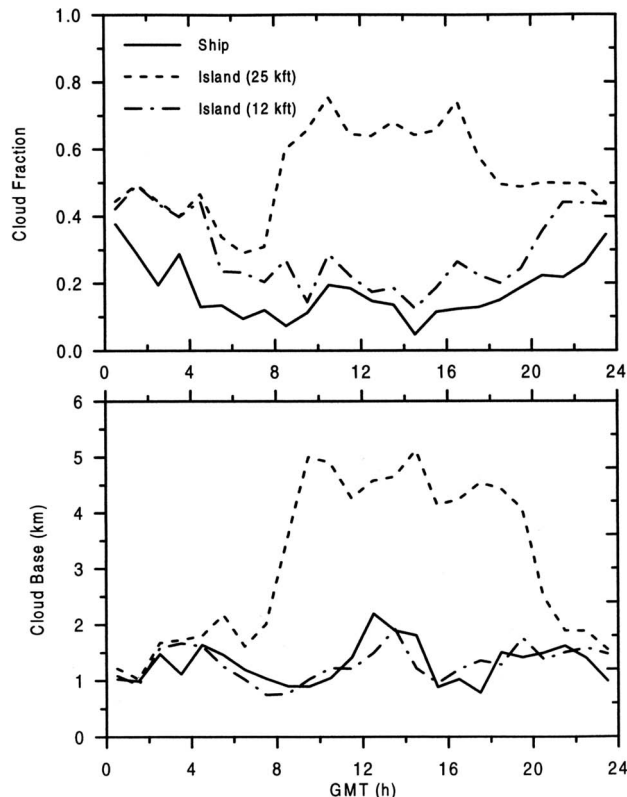


FIG. 13. Cloud fraction (top) and base (bottom) as a function of time of day, as measured by the ship's ceilometer (solid) and the island ceilometer (dashed), for 24 March–2 April 1996. The asymmetrically dashed curve is for island ceilometer data processed to 3.66-km altitude (12 000 ft) while the evenly dashed curve is for the same ceilometer processed to 7.62 km (25 000 ft). The ship's ceilometer acquired data only to 3.66 km. Local noon is approximately 0210 UTC.

at higher altitudes. The multitude of upwelling and downwelling radiometric measurements, and the accompanying aerosol and water vapor data, will undoubtedly help improve AVHRR products.

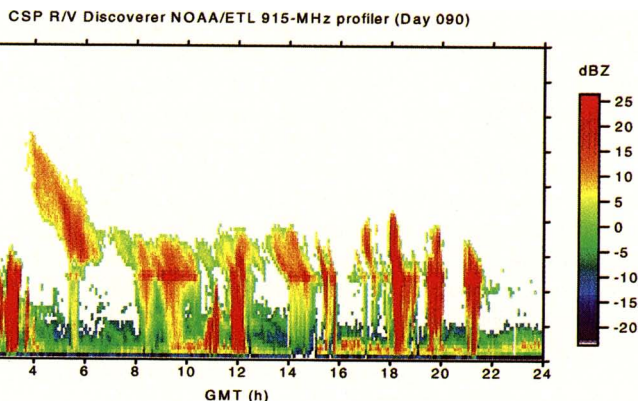
Because we experienced both typical and atypical atmospheric conditions, from clear and dry with light winds, to disturbed, unstable, and wet during the genesis of a tropical cyclone, we will be able to better parameterize fluxes, aerosols, and clouds across a broad range of conditions in climate models. We also have a small sample of data (10 days) to help determine if large landmasses near Manus Island, or the island itself, affect CART measurements.

While the overall campaign was a large success, there were nonetheless some disappointments. The sun photometer did not perform as well as anticipated, and the lidar systems failed prematurely. The cloud radar seldom operated with both frequencies simulta-

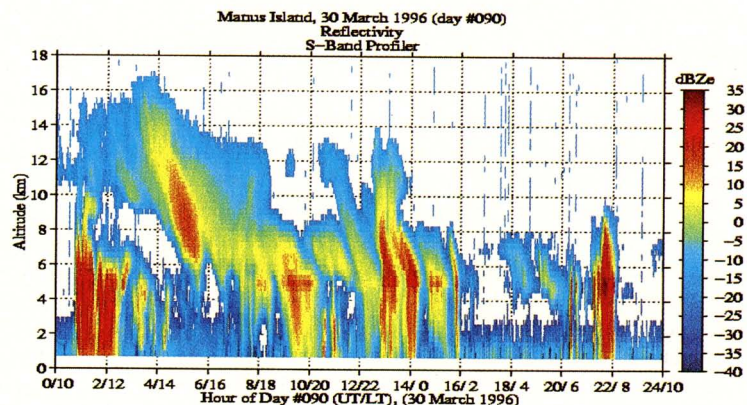
neously. Thus, the quantity of data from several of the center-piece instruments was not as large as hoped, reducing the number of hours available for multisensor synergism. Also, the instrument complement on Manus Island was considerably smaller than originally planned, because of delays in deploying the first ARCS container of standard DOE/ARM instruments.

Plans are for PIs to continue to analyze data and to hold a special session at the 1997 AGU Fall Meeting to present new findings. A similar mission for 1999 is being considered, to build on CSP findings and to better compare shipboard measurements with a complete set of ARM/ARCS instrumentation that will be on Nauru Island in 1999, in contrast to the incomplete set that was on Manus Island during CSP. The Nauru mission will be more comprehensive than CSP, with plans to include two ships and research aircraft. Also, Nauru Island is much smaller than Manus Island, and we expect significantly different island effects.

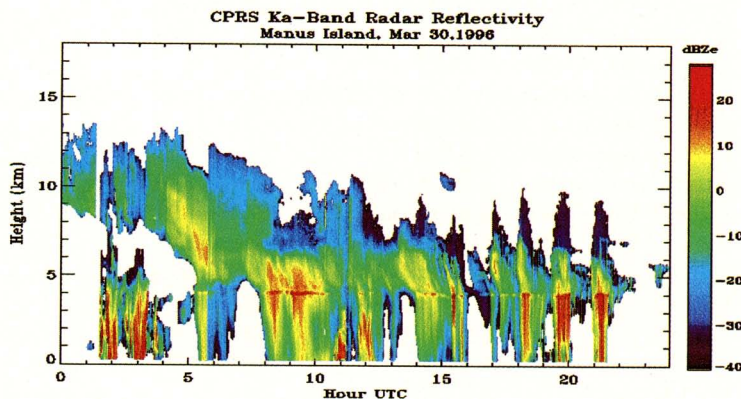
Acknowledgments. It is impractical to list as coauthors or to acknowledge everyone who made significant contributions to the CSP mission. John Herring and many others in NOAA Corps helped plan and coordinate the mission many months before any equipment was shipped, and Steve Piotrowicz of NOAA/OAR helped secure ship time for it. The entire ship's crew was unbelievably supportive during the mission, especially considering that the *Discoverer* was near the end of an extended deployment and was on its next to last mission, scheduled to be decommissioned after nearly 30 years of stalwart service to NOAA and our nation. The crew had to deal with a plethora of odd requests from many "rookie" atmospheric scientists on board. Mae Chu of InterConex and her agents David McNeil (Samoa) and Dick Pearse (Manus Island) provided indispensable aid in shipping and handling a great deal of sophisticated equipment throughout the mission. Mark Fiscus, Chuck Long, and Paul



(a)



(b)



(c)

FIG. 15. Simultaneously acquired reflectivity data from radars at three different frequencies: (a) 915 MHz, (b) 3 GHz, and (c) 33 GHz for 30 March 1996. The wind-profiling radar (a) and cloud radar (c) were on *Discoverer* while the precipitation radar (b) was on Manus Island. The Manus Island radar observed events slightly sooner because *Discoverer* was positioned 30 km downwind from the island.

Johnston helped coordinate activities on Manus Island with those of the ship's, and hosted a short but very helpful tour of island facilities. Kurt Nielson was injured while setting up the AVHRR receiver in Samoa, but still managed to get it operating before the ship departed. Dave Covert and Tim Bates helped bring the ACE aerosol instrumentation back on-line, and Gene Furness helped install rain gauges and disdrometers. Jim Churnside, Joe Shaw, Scott Abbott, and Jesse Leach helped install much of ETL's equipment in Samoa. Bill Porch provided S-band radar data and ceilometer data from Manus Island. John Bates and Wesley Berg

acquired GMS data and produced both images and video from it. Joan Hart was instrumental in providing analyses for the meteorological summary. David Welsh, Tom Glaess, Sandy King, and LingLing Zhang developed many of the capabilities for data management. Of course, all the CSP participants who are not listed as coauthors (Jeff Hare, Duane Hazen, Bill Eichinger, Larry Tellier, Mike Osborn, Scott Smith, Derek Coffman, Vladimir Kapustin, Lihua Li, Tom Saxen, Jorge Valero, Nick Nalli, Brian Osborne, and John Short) deserve special acknowledgment for their strong contributions, especially Duane Hazen who assisted the chief scientist greatly. Finally, we must thank Tom Ackerman and the rest of the ARM Science Team Executive Committee for having the vision to promote and support the ASTEX and CSP missions under Contract DE-AI02-92ER61366.

References

- Albrecht, B. A., D. A. Randall, and S. Nicholls, 1988: Observations of marine stratocumulus clouds during FIRE. *Bull. Amer. Meteor. Soc.*, **69**, 618–626.
- , C. S. Bretherton, D. Johnson, W. H. Schubert, and A. S. Frisch, 1995: The Atlantic Stratocumulus Transition Experiment—ASTEX. *Bull. Amer. Meteor. Soc.*, **76**, 889–904.
- Bjerknes, J., L. J. Allison, E. R. Kreins, F. A. Godshall, and G. Warnecke, 1969: Satellite mapping of the Pacific tropical cloudiness. *Bull. Amer. Meteor. Soc.*, **50**, 313–322.
- Bradley, E. F. and R. A. Weller, Eds., 1997: Fourth Workshop of the TOGA COARE Air–Sea Interaction (FLUX) Working Group. TOGA COARE Tech. Rep., 61 pp. [Available from TOGA COARE International Project Office, UCAR, P.O. Box 3000, Boulder, CO 80307-3000.]
- Browning, K. A., 1994: Survey of perceived priority issues in the parameterizations of cloud-related processes in GCMs. *Quart. J. Roy. Meteor. Soc.*, **120**, 483–487.
- Cess, R. D., and Coauthors, 1995: Absorption of solar radiation by clouds: Observations versus models. *Science*, **267**, 496–499.
- Chertock, B., C. W. Fairall, and A. B. White, 1993: Surface-based measurements and satellite retrievals of broken cloud properties in the equatorial Pacific. *J. Geophys. Res.*, **98**, 18 489–18 500.
- Chou, M.-D., A. Arking, J. Otterman, and W. L. Ridgeway, 1995: The effect of clouds on atmospheric absorption of solar radiation. *Geophys. Res. Lett.*, **22**, 1885–1888.
- Cooper, D. I., W. Eichinger, R. Ecke, J. Kao, J. Reisner, and L. Tellier, 1997: Initial investigations of microscale cellular convection in an equatorial marine atmospheric boundary layer revealed by lidar. *Geophys. Res. Lett.*, **24**, 45–48.
- Ecklund, W. L., P. E. Johnston, J. M. Warnock, W. L. Clark, and K. S. Gage, 1995: An S-band profiler for tropical precipitation studies. Preprints, *27th Conf. on Radar Meteorology*, Vail, CO, Amer. Meteor. Soc., 335–336.
- Evans, W. F. J., C. Reinhart, and E. Purckrin, 1995: A ground-based measurement of the anomalous cloud absorption effect. *Geophys. Res. Lett.*, **22**, 2135–2138.
- Fairall, C. W., E. F. Bradley, D. P. Rogers, J. B. Edson, and G. S. Young, 1996a: Bulk parameterization of air–sea fluxes in TOGA COARE. *J. Geophys. Res.*, **101**, 3747–3767.
- , —, J. S. Godfrey, G. A. Wick, J. B. Edson, and G. S. Young, 1996b: Cool skin and warm layer effects on the sea surface temperature. *J. Geophys. Res.*, **101**, 1295–1308.
- , A. B. White, J. B. Edson, and J. E. Hare, 1997: Integrated shipboard measurements of the marine boundary layer. *J. Atmos. Oceanic Technol.*, **14**, 338–359.
- Frisch, A. S., C. W. Fairall, and J. B. Snider, 1995: On the measurement of stratus cloud and drizzle parameters with a K_a -band Doppler radar and a microwave radiometer. *J. Atmos. Sci.*, **52**, 2788–2799.
- Gill, A. E., 1980: Some simple solutions for heat-induced tropical circulation. *Quart. J. Roy. Meteor. Soc.*, **106**, 447–462.
- Graham, N. E., and T. P. Barnett, 1987: Sea surface temperature, surface wind divergence, and convection over tropical oceans. *Science*, **238**, 657–659.
- Han, Y., J. A. Shaw, J. H. Churnside, P. D. Brown, and S. A. Clough, 1997: Infrared spectral radiance measurements in the tropical Pacific. *J. Geophys. Res.*, **102** (D4), 4353–4356.
- Hendon, H. H., and B. Liebmann, 1994: Organization of convection within the Madden–Julian oscillation. *J. Geophys. Res.*, **99**(D4), 8073–8083.
- Hogg, D. C., F. O. Guiraud, J. B. Snider, M. T. Decker, and E. R. Westwater, 1983: A steerable dual-channel microwave radiometer for measurement of water vapor and liquid in the troposphere. *J. Climate Appl. Meteor.*, **22**, 789–806.
- Jacobson, M. D., and W. N. Nunnelee, 1997: Design and performance of a spinning flat reflector for millimeter-wave radiometry. *IEEE Trans. Geosci. Remote Sens.*, **35**, 464–468.
- Kalnay, E., and Coauthors, 1996: The NCEP/NCAR 40-year reanalysis project. *Bull. Amer. Meteor. Soc.*, **77**, 437–471.
- Knuteson, R. O., F. A. Best, P. Minnett, H. E. Revercomb, and W. L. Smith, 1997: High spectral resolution infrared observations in the tropical western Pacific using a marine atmospheric emitted radiance interferometer (MAERI). Preprints, *Ninth Conf. on Atmospheric Radiation*, Long Beach, CA, Amer. Meteor. Soc., 180–183.
- Knutson, T. R., and K. M. Weickmann, 1987: 30–60 day atmospheric oscillations: Composite life cycles of convection and circulation anomalies. *Mon. Wea. Rev.*, **115**, 1407–1436.
- Lau, K.-M., and P. H. Chan, 1985: Aspects of the 40–50 day oscillation during northern winter as inferred from outgoing longwave radiation. *Mon. Wea. Rev.*, **113**, 1889–1909.
- Madden, R. A., and P. R. Julian, 1972: Description of global-scale circulation cells in the tropics with a 40–50 day period. *J. Atmos. Sci.*, **29**, 1109–1123.
- Nakazawa, T., 1988: Tropical super clusters within intraseasonal variations over the western Pacific. *J. Meteor. Soc. Japan*, **66**, 823–839.
- Quinn, P. K., V. N. Kapustin, T. S. Bates, and D. S. Covert, 1996: Chemical and optical properties of marine boundary layer aerosol particles of the mid-Pacific in relation to sources and meteorological transport. *J. Geophys. Res.*, **101**, 6931–6951.
- Ramanathan, V., B. Subasilar, G. J. Zhang, W. Conant, R. D. Cess, J. T. Kiehl, H. Grassl, and L. Shi, 1995: Warm pool heat budget and shortwave cloud forcing: A missing physics? *Science*, **267**, 499–503.
- Randall, D. A., J. A. Coakley, C. W. Fairall, R. A. Kropfli, and D. H. Lenschow, 1984: Outlook for research on subtropical marine stratiform clouds. *Bull. Amer. Meteor. Soc.*, **65**, 1290–1301.
- Reynolds, R. M., and S. Smith, 1997: The R/V *Discoverer* cruise to Manus Island—The BNL Portable Radiation Package (PRP) evaluation. Rep. 64333, 45 pp. [Available from Brookhaven National Laboratory, Upton, NY 11973.]

- Sekelsky, S. M., and R. E. McIntosh, 1996: Cloud observations with a polarimetric 33-GHz and 95-GHz radar. *J. Meteor. Atmos. Phys.*, **58**, 123–140.
- Shaw, J. A., J. B. Snider, J. H. Churnside, and M. D. Jacobson, 1995: Comparison of infrared atmospheric brightness temperatures measured by a Fourier transform spectrometer and a filter radiometer. *J. Atmos. Oceanic Technol.*, **12**, 1124–1128.
- Sheppard, B. E., and P. I. Joe, 1994: Comparison of raindrop size distribution measurements by a Joss–Waldvogel disdrometer, a PMS 2DG spectrometer, and a POSS Doppler radar. *J. Atmos. Oceanic Technol.*, **11**, 874–887.
- Smith, W. L., and Coauthors, 1996: Observations of the infrared radiative properties of the ocean: Implications for the measurement of sea surface temperature via satellite remote sensing. *Bull. Amer. Meteor. Soc.*, **77**, 41–51.
- Soloviev, A. V., and P. Schluskel, 1996: Evolution of cool skin and direct air–sea gas transfer coefficient during daytime. *Bound.-Layer Meteor.*, **77**, 45–68.
- Soumi, V. E., L. A. Sromovsky, and J. R. Anderson, 1996: Measuring ocean–atmosphere heat flux with a few in-situ sensors. Preprints, *Eighth Conf. on Air–Sea Interaction*, Atlanta, GA, Amer. Meteor. Soc., 36–42.
- Stokes, G. M., and S. E. Schwartz, 1994: The Atmospheric Radiation Measurement (ARM) program: Programmatic background and design of cloud and radiation testbed. *Bull. Amer. Meteor. Soc.*, **75**, 1201–1221.
- Waliser, D. E., N. E. Graham, and C. Gautier, 1993: Comparison of the highly reflective cloud and outgoing longwave radiation datasets for use in estimating tropical deep convection. *J. Climate*, **6**, 331–353.
- Wang, T. I., K. B. Earnshaw, and R. S. Lawrence, 1978: Simplified optical path-averaged rain gauge. *Appl. Opt.*, **17**, 384–390.
- Webster, P. J., and R. Lukas, 1992: TOGA COARE: The Coupled Ocean–Atmosphere Response Experiment. *Bull. Amer. Meteor. Soc.*, **73**, 1377–1416.
- , C. A. Clayson, and J. A. Curry, 1996: Clouds, radiation, and the diurnal cycle of sea surface temperature in the tropical western Pacific. *J. Climate*, **9**, 1712–1730.
- White, A. B., C. W. Fairall, and J. B. Snider, 1995: Surface-based remote sensing of marine boundary-layer cloud properties. *J. Atmos. Sci.*, **52**, 2827–2838.
- Young, G. S., D. R. Ledvina, and C. W. Fairall, 1992: Influence of precipitating convection on the surface energy budget observed during a Tropical Ocean Global Atmosphere pilot cruise in the tropical western Pacific Ocean. *J. Geophys. Res.*, **97**, 9595–9603.
- , S. M. Perugini, and C. W. Fairall, 1995: Convective wakes in the equatorial Pacific during TOGA COARE. *Mon. Wea. Rev.*, **123**, 110–123.
- Zhang, G. J., and R. L. Grossman, 1996: Surface evaporation during the Central Equatorial Pacific Experiment: A climate scale perspective. *J. Climate*, **9**, 2522–2537.
- , V. Ramanathan, and M. J. McPhaden, 1995: Convective–evaporative feedback in the equatorial Pacific. *J. Climate*, **8**, 3040–3051.

Stochastic Lagrangian Models of Turbulent Diffusion

Meteorological Monograph No. 48

by Howard C. Rodean

Until now, atmospheric scientists have had to learn the mathematical machinery of the theory of stochastic processes as they went along. With this monograph, atmospheric scientists are given a basic understanding of the physical and mathematical foundations of stochastic Lagrangian models of turbulent diffusion. The culmination of four years of research, *Stochastic Lagrangian Models of Turbulent Diffusion* discusses a historical review of Brownian motion and turbulent diffusion; applicable physics of turbulence; definitions of stochastic diffusion; the Fokker–Planck equation; stochastic differential equations for turbulent diffusion; criteria for stochastic models of turbulent diffusion; turbulent diffusion in three dimensions; applications of Thompson's "simplest" solution; application to the convective boundary layer; the boundary condition problem; and a parameterization of turbulence statistics for model inputs.

©1996 American Meteorological Society. Hardbound, B&W, 84 pp., \$55 list/\$35 members (includes shipping and handling). Please send prepaid orders to: Order Department, American Meteorological Society, 45 Beacon St., Boston, MA 02108-3693.

**American
Meteorological
Society**

HANDS-ON

METEOROLOGY

*Stories, Theories, and
Simple Experiments*

Zbigniew Sorbjan

Hands-on Meteorology presents the subject of atmospheric science in an exciting, intriguing, and entertaining way. Utilizing a "hands-on" approach, readers perform simple experiments that demonstrate concepts of basic meteorology: air pressure, heat, temperature, moisture, and wind. The experiments use common, everyday, inexpensive materials such as candles, bottles, cans, and balloons.

Hands-on Meteorology also contains meteorological anecdotes, historical narratives, references to important cultural events, and biographical sketches of prominent scientists.

Hands-on Meteorology is addressed to all those who are enthusiastic about learning and teaching about the atmosphere, weather, and climate and should prove entertaining for readers of all ages.

©1996 American Meteorological Society. Softcover, B&W, 306 pp., \$21.95 list/\$16.00 member (including shipping and handling). **Please send prepaid orders to:** Order Department, American Meteorological Society, 45 Beacon St., Boston, MA 02108-3693.

Project ATMOSPHERE is the educational initiative of the American Meteorological Society to foster the teaching of atmospheric topics across the curriculum grades K-12. It is a unique partnership between scientists and teachers with the ultimate goal of attracting young people to further studies in science, mathematics, and technology.



Project ATMOSPHERE
AMERICAN METEOROLOGICAL SOCIETY